Geophysical Research Letters

RESEARCH LETTER
10.1029/2024GL111502

Influence of Indian Ocean Tropical Cyclones on the Development of the Madden-Julian Oscillation in December 2011

Suyang Pei[1] and **Toshiaki Shinoda**[1]

[1]Department of Physical and Environmental Sciences, Texas A&M University-Corpus Christi, Corpus Christi, TX, USA

Key Points:

- The 2011 Dec. Madden-Julian Oscillation (MJO) initiation differs from most other MJOs due to modulation by two tropical cyclones (TCs) in the southern Indian Ocean (IO)
- TC-induced zonal and meridional circulations sustain a dry air band in 10°S-Eq, inhibiting convection in the southern equatorial IO
- Convection develops eastward within Eq-10°N during TC-active period and evolves into the MJO after the TCs dissipate

Supporting Information:

Supporting Information may be found in the online version of this article.

Correspondence to:

S. Pei,
suyang.pei@tamucc.edu

Citation:

Pei, S., & Shinoda, T. (2025). Influence of Indian Ocean tropical cyclones on the development of the Madden-Julian Oscillation in December 2011. *Geophysical Research Letters*, *52*, e2024GL111502. https://doi.org/10.1029/2024GL111502

Received 19 JUL 2024
Accepted 4 DEC 2024

Abstract Previous studies demonstrate that the Madden-Julian Oscillation (MJO) modulates tropical cyclone (TC) activity over various locations worldwide. Since TCs are associated with anomalous large-scale circulations, they can influence the development of the MJO. However, the impact of TC on the MJO has not been thoroughly examined. This study investigates the influence of TC-associated processes on the MJO development based on the analysis of a case observed during the Dynamics of the Madden-Julian Oscillation field campaign. During the suppressed phase before the December 2011 MJO initiation, two TCs were active in the southern Tropical Indian Ocean (TIO). A dry air band within 10°S-Eq is sustained by TC-induced horizontal advection and descent, inhibiting large-scale convection in the southern equatorial IO. Consequently, convection is triggered and develops only in the northern TIO around Eq-10°N. The MJO initiates as convection develops south of the equator after the TCs dissipate.

Plain Language Summary The Madden-Julian Oscillation (MJO) is an eastward-moving disturbance, characterized by variations in cloud cover, rainfall, and wind patterns, with a period of 30–60 days. It travels along the equator, significantly influencing extreme weather events worldwide, including tropical cyclone (TC) activity. TCs can, in turn, potentially influence the development of the MJO through their associated strong anomalous large-scale circulation. However, this impact has not been systematically investigated in previous studies. This study demonstrates the impact of TCs on the initiation of an MJO event over the Tropical Indian Ocean (TIO), using data collected from an international field campaign. In early December of 2011, two TCs were observed in the southern TIO. They induced descending motion and strong eastward winds over the southern equatorial IO (EIO), sustaining a dry air band that inhibits large-scale convection over this region. As a result, convection develops only in the northern EIO during the presence of TCs. After TCs dissipate, convective systems extend south of the equator, organizing into a large-scale convective envelope, indicating the initiation of the MJO.

1. Introduction

The Madden-Julian Oscillation (MJO; Madden & Julian, 1971, 1972) is the dominant mode of the tropical atmospheric intraseasonal variability during boreal winter and spring (e.g., Jiang et al., 2020). Many previous studies have demonstrated that the MJO strongly modulates tropical cyclone (TC) activity across various ocean basins throughout its life cycle (e.g., Aiyyer & Molinari, 2008; Balaguru et al., 2021; Barrett & Leslie, 2009; Camargo et al., 2008; Chand & Walsh, 2010; Hall et al., 2001; Hansen et al., 2024; Klotzbach & Blake, 2013; Liebmann et al., 1994; Maloney & Hartmann, 2000; Ramsay et al., 2012; Sobel & Maloney, 2000; Ventrice et al., 2011). It also influences the rapid intensification of TCs (e.g., Aberson & Kaplan, 2020; Klotzbach, 2012) and their landfall (Klotzbach et al., 2023).

In the Tropical Indian Ocean (TIO), while the MJO enhances the TC activity during its convectively active phase over the basin (e.g., Bessafi & Wheeler, 2006; Ho et al., 2006; Krishnamohan et al., 2012), TCs could also influence the MJO due to their associated anomalous large-scale circulation. Several previous studies have investigated the influence of westward propagating waves, including the equatorial Rossby (ER) waves, the mixed Rossby-gravity (MRG) waves and the tropical depression (TD)-type disturbances, on the development of MJO (e.g., S. Chen et al., 2015; Muraleedharan et al., 2015; Takasuka & Satoh, 2020; Yasunaga et al., 2010). For instance, Kerns and Chen (2014) suggest that equatorial dry air intrusion from subtropics driven by the circulations associated with westward-propagating waves suppress convection on the west side of the November 2011 MJO (referred to as "Nov. MJO" hereafter), facilitating its eastward propagation. TCs are associated with

more intense anomalous circulation than the westward-propagating waves. Nevertheless, the impact of TCs on the MJO remains unclear. In particular, previous research has not explored how TCs influence the development of convection that ultimately leads to MJO deep convection.

This study investigates the potential impact of TCs on the development of the MJO, focusing on a case observed in December 2011 (referred to as "Dec. MJO" hereafter) during the Dynamics of the Madden-Julian Oscillation (DYNAMO) field campaign (Yoneyama et al., 2013). In the convectively suppressed phase preceding the Dec. MJO initiation, two TCs developed in the southern TIO, substantially influencing convection development over the equatorial IO (EIO). For typical MJO events initiated in the IO, convection begins in the Southwest TIO (e.g., Takasuka & Satoh, 2020), intensifies and shifts toward the equator while propagating eastward across the region (e.g., Zhao et al., 2013). However, for the Dec. MJO event, convection is initially triggered in the northwestern EIO (NW-EIO), with subsequent development also occurring north of the equator. After the dissipation of TCs, the MJO initiates over the central EIO (C-EIO) with convection extending south of the equator. This study emphasizes the role of TC-associated processes in controlling large-scale circulation and moisture distribution, which significantly influences the convection development leading to the MJO initiation.

2. Data and Methodologies

Large-scale convection associated with the MJO is described using the daily NOAA Interpolated Outgoing Longwave Radiation (OLR; Lee et al., 2014) data with a 2.5° horizontal resolution. Precipitation is examined using the NOAA Climate Data Record of Climate Prediction Center Morphing Technique (CMORPH) High-Resolution Global Precipitation Estimates version 1 (Xie et al., 2019), which provides daily and hourly bias-corrected reprocessed satellite precipitation on a 0.25° horizontal grid. Surface winds are described using the Cross-Calibrated Multi-Platform (CCMP; Atlas et al., 2011; Wentz et al., 2015) gridded surface vector wind data, which are available 6-hourly on a 0.25° global grid. The International Best Track Archive for Climate Stewardship (IBTrACS; Knapp et al., 2010) data are used to track the TCs. The atmospheric circulation and moisture distribution are analyzed using the ECMWF Reanalysis v5 (ERA5; Hersbach et al., 2020), which provides hourly data on 37 pressure levels with a 0.25° horizontal resolution. These data agree well with the DYNAMO sounding data (Johnson & Ciesielski, 2013; Johnson et al., 2019; Figure S1 in Supporting Information S1). The sea surface temperature (SST) variation is displayed daily on a 0.25° horizontal grid using the NOAA Optimum Interpolated SST version 2.0 (OI SSTv2; Reynolds et al., 2007).

Previous studies suggest that westward-propagating equatorial waves significantly influence convection development over the TIO (e.g., Fukutomi & Yasunari, 2013; Takasuka & Satoh, 2020). However, isolating individual modes of these waves (e.g., MRG, ER and TD-type disturbances) can be challenging, as they often transition into other wave modes due to background flow variations (e.g., G. Chen & Huang, 2009; Kerns & Chen, 2014; Liebmann & Hendon, 1990; Roundy & Frank, 2004). Consequently, this study examines the convection development north of the equator primarily in the context of sub-monthly scale waves, applying a band-pass Lanczos filter (Duchon, 1979) with a window of 2–30-day to extract their signals. Additionally, the role of MRG and TD-type disturbances (referred to as MRGTD thereafter due to their continuous presence on the wavenumber frequency spectra) and ER waves in triggering convection are examined by applying band-pass filters for the 2–10-day and 10–30-day periods, respectively. All anomalies are computed with respect to the 2011 November-December mean. Variables averaged within 1,000–800 hPa represent their values in the lower troposphere (LTr).

3. Results

3.1. TCs in the Convectively Suppressed Phase of the December 2011 MJO

The eastward propagation of large-scale deep convection associated with the 2011 Nov. and Dec. MJOs over the EIO is evident from the negative OLR anomaly shown in Figure 1a. The Nov. MJO initiates in the southwestern EIO (SW-EIO) around 50°E and has been extensively analyzed in previous studies (e.g., S. Chen et al., 2015; Kerns & Chen, 2014; Moum et al., 2014; Powell & Houze, 2015; Shinoda et al., 2013; Takasuka et al., 2019, 2021). Unlike the Nov. MJO, deep convection of the Dec. MJO initiates on December 16 in the C-EIO, indicated by the significantly enhanced apparent heating source and moisture sink profiles (Yanai et al., 1973) derived from the DYNAMO sounding array data (Figure S2 in Supporting Information S1; Ruppert & Johnson, 2015) and the OLR anomaly (Figure 1a).

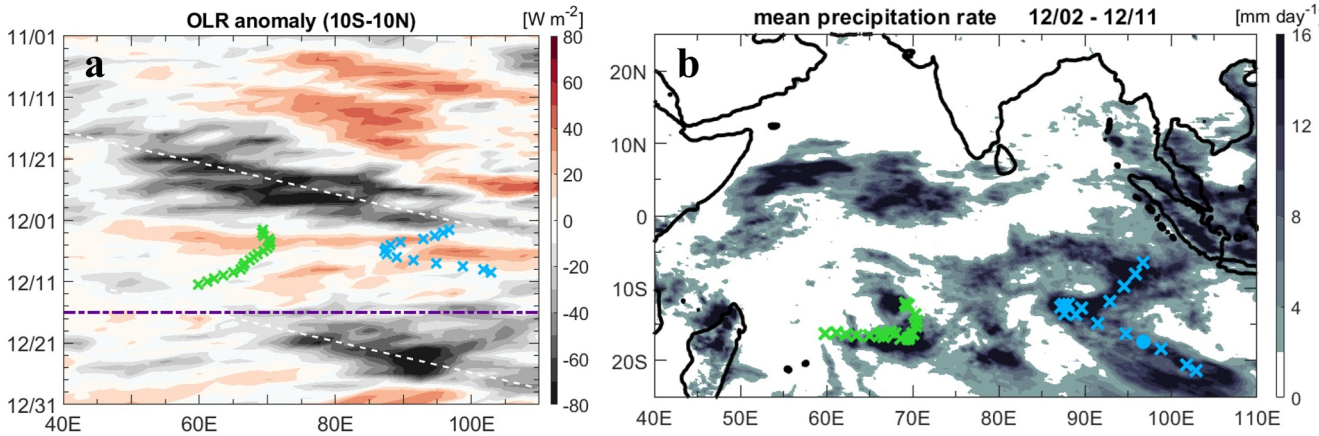

Figure 1. (a) Longitude-time Hovmöller diagram of OLR anomaly averaged between 10°S–10°N. The green (blue) crosses display the longitudinal locations of wTC (eTC) during its active period. The white dashed lines indicate eastward propagation of 5 m s^{-1}. The purple dashed dotted line marks the Dec. Madden-Julian Oscillation initiation date December 16. (b) Mean precipitation rate during the TC-active period 02–11 December 2011. The green (blue) crosses represent the locations of wTC (eTC) every 12-hr during this period. The green (blue) circle indicates the location where wTC (eTC) reaches its maximum sustained wind speed.

In the convectively suppressed phase prior to the Dec. MJO initiation, two TCs are active in the southern TIO (Figure 1a). The eastern TC (eTC) was first detected near 96°E, 5°S, categorized as a moderate tropical storm. It is active during Dec. 02–10, reaching its maximum sustained wind speed (V_{max}) of ∼48.9 m s^{-1} on Dec. 08. The western TC (wTC) was first recorded around 70°E, 10°S, categorized as a tropical depression during Dec. 02–11 with a V_{max} of ∼17.5 m s^{-1} attained on Dec. 06. The wTC develops from some TD-type disturbances formed when the Nov. MJO propagates across the central IO (Kerns & Chen, 2014). The eTC forms from an ER gyre that spins off the Nov. MJO when its convection center enters the Maritime Continent (MC) (Figure 2a1). Their paths are shown in Figure 1b along with the mean precipitation during their active period. Heavy rainfall areas are found surrounding the TCs and in the NW-EIO, indicating the development of convection in these regions. It should be noted that the track and intensity of the two TCs are strongly modulated by the location and strength of the subtropical high over the southern IO during this period (not shown).

3.2. Impact of TCs on Large-Scale Atmospheric Circulation

In the TIO, the December climatological mean winds are generally strong northeasterlies over the Arabian Sea and the Bay of Bengal (BOB) associated with the winter monsoon. These winds weaken toward the equator and turn to weak westerlies south of the equator (e.g., Beal et al., 2013). However, during the TC-active period (Dec. 02–11), strong westerlies persist in the southern EIO (S-EIO; 10°S-Eq, Figure 2a) due to the influence of TCs, as demonstrated by the analysis in this section.

The wTC sustains strong anomalous westerlies within 55°E–75°E, 10°S-Eq (Figure 2b1). This is further evidenced by the time-latitude Hovmöller diagram of zonally averaged LTr anomalous wind speed, where enhanced anomalous westerlies (≥3 m s^{-1}) closely track the movement of the wTC (Figure 2b2). In contrast to the limited poleward movement of the wTC, the eTC initiates near the equator and moves poleward, spanning a large meridional area (Figure 2b1). On Dec. 02, the equatorial winds between 80°E and Sumatra are strengthened by a pair of ER gyres generated west of the Nov. MJO deep convection (Figure 2a1). While the northern gyre quickly dissipates, the southern gyre transitions into the eTC. The eTC intensifies as it moves poleward from the equatorial area (Figures 2a2 and 2a3), reinforcing anomalous westerlies in the eastern EIO (E-EIO) within 10°S–5°S (Figure 2b3). In early December, the large-scale Walker circulation linked to the Nov. MJO deep convection over the MC also supports the LTr anomalous westerlies in the S-EIO. However, as the eTC approaches the wTC on Dec. 05 (Figures 2a1 and 2a2), strong convection develops between them, disrupting the MJO-linked large-scale Walker circulation by inducing a zonal circulation within 60°E–90°E, 10°S-Eq (Figure S3a in Supporting Information S1). During Dec. 08–11, westerlies in the S-EIO remain strong despite the Nov. MJO weakening over the MC (Figure S3b in Supporting Information S1), indicating these westerlies are primarily sustained by the TCs rather than the large-scale Walker circulation.

10.1029/2024GL111502

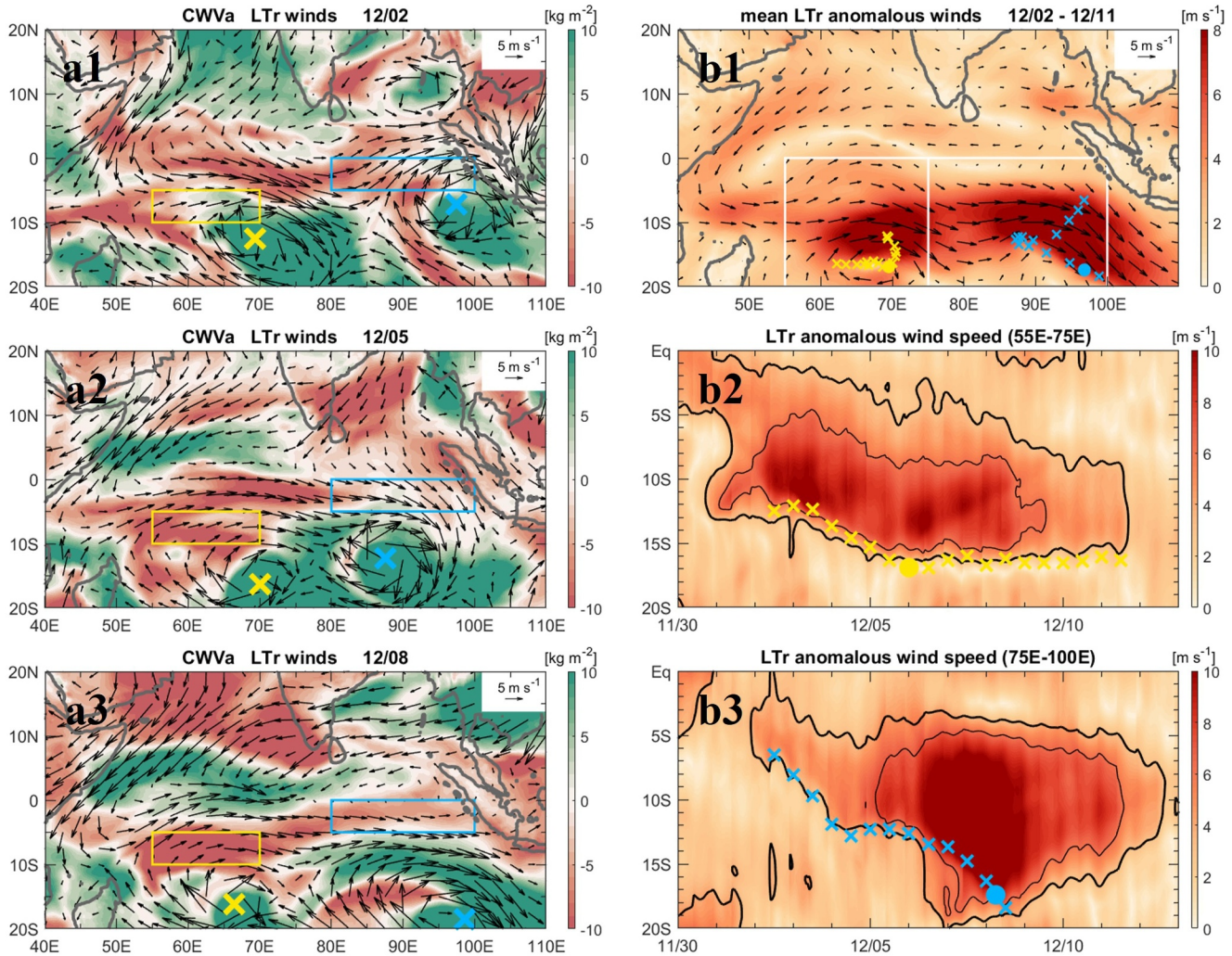

Figure 2. Daily mean column water vapor anomaly (CWVa; shading) and lower troposphere (LTr) winds (vectors) over the Tropical Indian Ocean (TIO) on (a1) Dec. 02; (a2) Dec. 05; (a3) Dec. 08. The yellow (blue) cross indicates the center of the wTC (eTC) on each day. Green (red) shading indicates areas with anomalous moist (dry) condition. The yellow (blue) box represents the western (eastern) part of the dry air band, where area-averaged column-integrated moisture budget is further analyzed (see Figure 3 below). (b1) Mean LTr anomalous winds (vectors) and wind speed (shading) over the TIO during the TC-active period. The white boxes are the regions where zonally averaged anomalous winds are examined. (b2) Time-latitude Hovmöller diagram of LTr anomalous wind speed (shading) and contours of zonal winds at 3 m s^{-1} (thick black lines) and 6 m s^{-1} (thin black lines) averaged between 55°E–75°E, indicated by the left box in (b1) during 30 Nov.–13 Dec. 2011. (b3) is the same as (b2) except averaged between 75°E–100°E, indicated by the right box in (b1). The yellow (blue) crosses represent the latitudinal path of wTC (eTC) at 12-hr intervals, while the circle indicates the time and latitude corresponding to the TC's maximum sustained wind speed.

3.3. Impact of TCs on Moisture Distribution in the Southern Equatorial IO

Climatologically in December, the weak westerlies within 10°S-Eq align closely with the moist Intertropical Convergence Zone (ITCZ), where the northeasterly and southeasterly monsoons converge. The TC-associated anomalous circulation significantly alters this moisture distribution over the TIO, making the initiation of the Dec. MJO event distinct from typical MJO events. Kerns and Chen (2014) suggest that equatorial dry air intrusion from the subtropics shuts down the Nov. MJO convection over the TIO. This equatorial dry air intrusion is evident on Dec. 02, forming a dry air band (DAB) along the EIO (Figure 2a1), which persists until the Dec. MJO initiation (Figure S4 in Supporting Information S1). In addition to supplying subtropical dry air to the equatorial area, TCs play a critical role in maintaining the DAB within 10°S-Eq, as shown in the following analysis.

The western part of the DAB (wDAB; 50°E–75°E, 10°S-Eq) is drier than the eastern part (east of ~75°E, Figures 2a2 and 2a3) due to a more confined poleward movement of the wTC than the eTC. The zonal advection associated with the wTC-induced strong westerlies contributes primarily to reinforcing the wDAB, as indicated

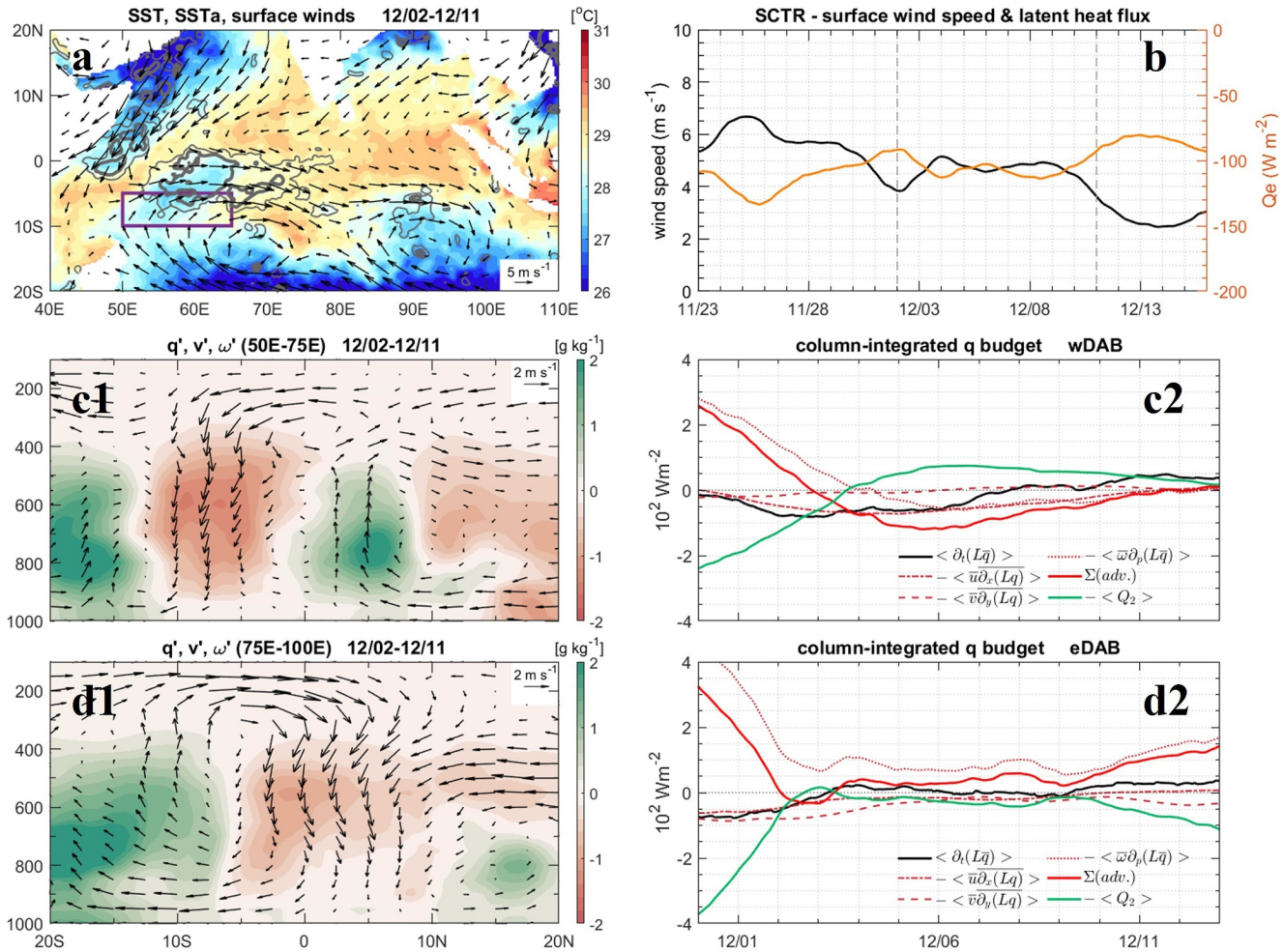

Figure 3. (a) Mean sea surface temperature (SST) (shading) and surface winds (vectors) averaged during the TC-active period (December 02–11). The thick (thin) contours indicate SST anomalies of 0.5°C (0.25°C). The purple box represents the Seychelles–Chagos Thermocline Ridge (SCTR) region (50°E–65°E, 10°S–5°S). (b) Time series of surface wind speed (black) and latent heat flux (orange) from November 23-December 15 averaged over the SCTR region as indicated by the purple box area in panel (a). The time between the two vertical dashed lines represents the TC-active period. (c1) Meridional-vertical contour of mean anomalous specific humidity (q′; shading) and meridional circulation (v′, ω′; vectors) averaged over 50°E–75°E during TC-active period. The vertical velocity ω′ has been multiplied by a factor of 1,000 for viewing purposes. (c2) Time series of area-averaged column-integrated moisture budget over the central wDAB area (55°E–70°E, 10°S–5°S; yellow box in Figure 2a) during 30 Nov.–13 Dec. 2011. The overbar indicates area average, the bracket represents vertical integration from 1,000 hPa to 100 hPa. The solid black line is the moisture tendency term; the solid red line is the total moisture advection term, which is the summation of zonal (red dashed dotted line), meridional (red dashed line) and vertical (red dotted line) components. The solid green line represents the apparent moisture source term, which is the difference between surface evaporation and precipitation. The black dotted line displays zero moisture change. A 5-day running mean is applied to smooth the results. All terms shown are in units of 100 W m^{-2}. Refer to the Supporting Information S1 for a detailed derivation of each budget term. (d1) is the same as (c1) except averaged over 75°E–100°E. (d2) is the same as (c2) except over the central eDAB area (80°E–100°E, 5°S-Eq; blue box in Figure 2a).

by the area-averaged column-integrated moisture budget over the central wDAB area (55°E–70°E, 10°S–5°S) (Figure 3c2; refer to the Supporting Information S1 for a detailed derivation). Prior to Dec. 02, convection over the wDAB area weakens (Figure 2a1) due to the substantial drying caused by dry air intrusion through horizontal advection, with zonal advection playing a primary role. As the wTC strengthens and moves poleward to ∼15°S, zonal advection continues to dominate the drying of the wDAB. Additionally, the wDAB is sustained by a wTC-induced meridional circulation. The presence of DAB over the S-EIO allows convection to only develop north of the equator, indicated by the eastward extension of moist areas (Figure 2a; Section 3.4). The convective updraft in the NW-EIO, along with that of the wTC south of 10°S, creates a double-cell meridional circulation with strong descent over 10°S–5°S (Figure 3c1), further strengthening the wDAB as indicated by the negative vertical advection term (Figure 3c2). Note that the instantaneous convective updraft associated with the wTC is much stronger and narrower than that averaged over the TC-active period (Figure S5a in Supporting Information S1).

Meanwhile, although the wDAB is moistened by enhanced evaporation (Figure 3c2) due to the wTC-strengthened westerlies, this effect is weaker compared to the drying caused by zonal and vertical advection. After the wTC reached maximum sustained winds on Dec. 06, both advection and moisture source terms begin to decrease, with advection declining more rapidly. Consequently, the drying of the wDAB weakens. During Dec. 08–10, the wDAB is maintained by a balance between moistening through surface evaporation and drying from zonal and vertical advection. As the wTC dissipates on Dec. 11, the advection-driven drying ceases, and the wDAB begins to moisten by surface evaporation.

In addition to the anomalous atmospheric circulation associated with the wTC, anomalous SST distribution could further contribute to maintaining the wDAB. The wDAB extends over the Seychelles–Chagos Thermocline Ridge (SCTR) region (Figure 3a, purple box), which is the shallowest thermocline near the equator due to the year-round upwelling. As a result, the SST is sensitive to small changes of surface forcing and thermocline depth in this region (e.g., Hermes & Reason, 2008; Shinoda et al., 2017; Xie et al., 2002). During the TC-active period, the wTC supports strong surface winds over the SCTR region, maintaining enhanced evaporative cooling even after the Nov. MJO westerly wind bursts (Figure 3b). Also, the cyclonic circulation associated with the wTC strengthens the negative wind stress curl in this area, leading to stronger upwelling and an elevated thermocline (Figure S6 in Supporting Information S1). Coupled with the strong surface winds, this could enhance entrainment cooling through vertical mixing. These cooling processes result in a persistent cold SST (~28°C, with a negative SST anomaly >0.5°C) area within 50°E–65°E centered at ~5°S, extending northeastward toward the equator (Figure 3a). The relatively cold SST in this area could facilitate convective inhibition by slowing the remoistening process. Previous studies suggest that the MJO convective triggering occurs favorably over the SCTR region due to strong air-sea interactions (e.g., Rydbeck & Jensen, 2017; Webber et al., 2010, 2012; West et al., 2020). However, for the 2011 Dec. MJO, the cold SST caused by the wTC-induced wind forcing suppresses convective initiation over the SCTR region.

The eastern part of the DAB (eDAB; 75°E–100°E, 10°S-Eq) is weaker and experiences more variability than the wDAB, as the eTC travels more than 15° poleward and shifts its direction from southwestward to southeastward (Figure 1b). Consequently, the mechanism that sustains the eDAB differs from that of the wDAB. Before the TC-active period, equatorial dry air intrusion by horizontal advection generates remarkable drying over the area as indicated by the moisture budget over the central eDAB area (80°E–100°E, 5°S-Eq; Figure 3d2). Meridional advection plays a greater role than zonal advection in drying the eDAB as dry air is largely transported by the eTC-associated southerlies (Figure 2a1). While the eTC moves southwestward toward the wTC, strong convection occurs, moistening the area between them. During Dec. 02–04, drying of the eDAB shifts to slightly moistening when the moisture sink term turns into a source term driven by decreased (increased) precipitation (evaporation). As the eTC approaches the wTC, convection develops southwest of the eDAB, further enhancing the moistening. Subsequently, following the southeastward movement of eTC, convection extends eastward within 10°S–5°S, separating the eDAB from the eTC and preventing further equatorial dry air intrusion from subtropics (Figures 2a2 and 2a3). During Dec. 05–08, despite weakened horizontal advection, the eDAB persists due to increased moisture sink term. Meanwhile, the northeastern EIO (NE-EIO) remains predominantly dry, which creates a meridional circulation with convective updraft south of the eDAB area and descent within 5°S–10°N (Figure 3d1; a much stronger and narrower instantaneous convective updraft associated with the eTC can be found in Figure S5b in Supporting Information S1). After Dec. 08, convection extends eastward from the NW-EIO into the NE-EIO (Figure 2a3), moistening the eDAB area from the north through increased vertical advection (Figure 3d2).

3.4. Convection Development in the Northern Equatorial IO During TC-Active Period

The TC-supported DAB inhibits development of large-scale convection in the S-EIO, allowing it to occur only in the northern EIO (N-EIO). On Dec. 02, a large moist area over the southern Arabian Sea, extending to 5°N, facilitates convective initiation in the NW-EIO (Figure 2a1). Convection initiates within 53°E–59°E, 5°N–10°N (Figure 4a1), driven by LTr meridional convergence caused by the equatorward deceleration of northeasterlies (Figure 2a1). The deacceleration occurs northwest to an anomalous counterclockwise circulation centered at 60°E on the equator (Figure 4b1). A pair of nearly symmetric anticyclonic gyres is evident in the sub-monthly scale winds (Figure 4c1), resembling the circulation structure of theoretical ER waves (e.g., Matsuno, 1966). The northern gyre, centered at 62°E, 7°N, generates southeasterlies south of the convection area, suggesting notable contribution of the ER waves to the convective initiation. This is further supported by examining the LTr winds

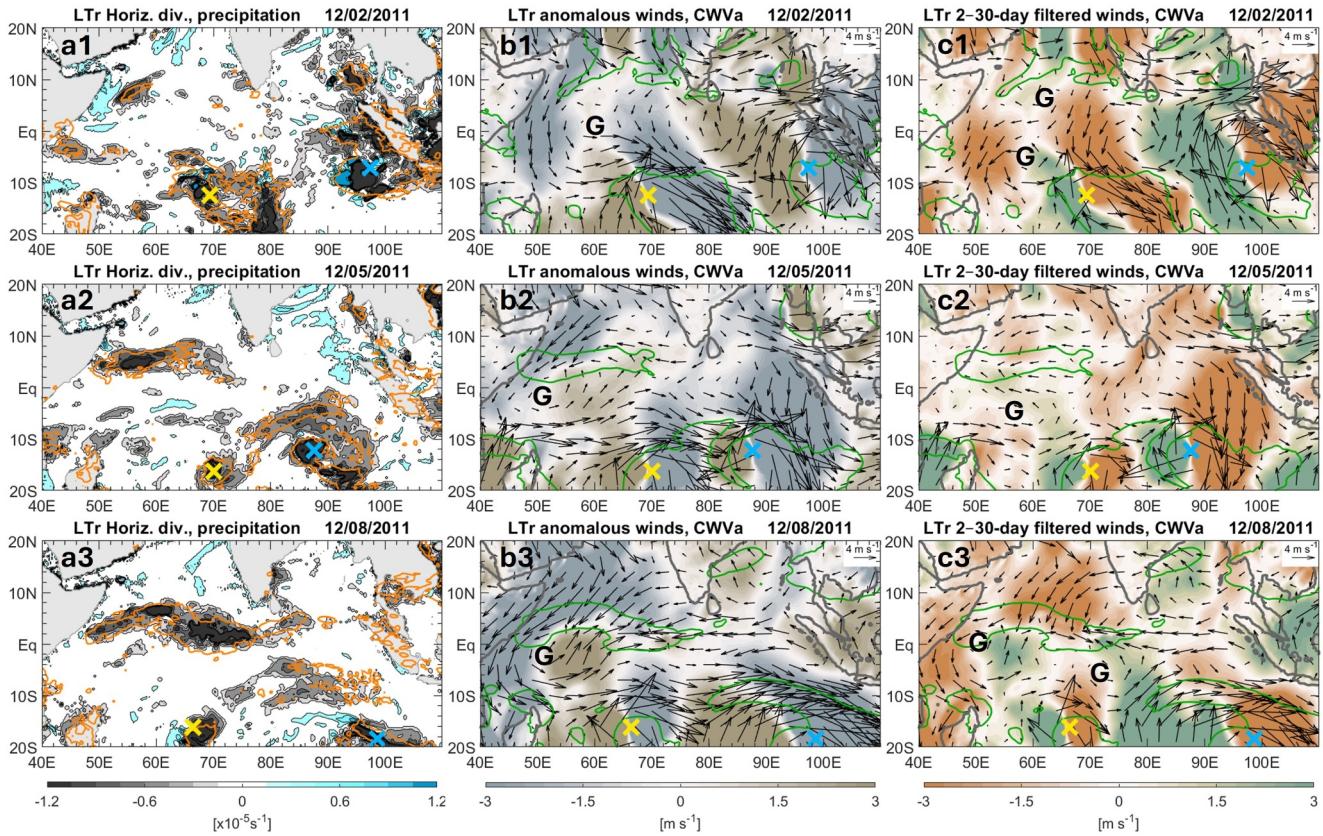

Figure 4. Daily mean horizontal convergence (shading in gray and black) in the lower troposphere (LTr) (only absolute values > 0.175×10^{-5} s^{-1} are shown) and precipitation of 8 mm day^{-1} (orange contours) on (a1) Dec. 02; (a2) Dec. 05; (a3) Dec. 08. (b1–b3) are the same as (a1–a3) except for the LTr anomalous winds (vectors, the vector size in the legend represents 4 m s^{-1}), anomalous meridional winds (shading, from −3 to 3 m s^{-1}) and CWVa contours of 6 kg m^{-2} (green lines); (c1–c4) are the same as (b1–b4) except for the LTr 2−30-day filtered winds. The location of the wTC (eTC) is indicated by a yellow (blue) cross on each day. The circulations associated with convection development in the NW-EIO are marked with the letter "G" at their approximate centers.

associated with the ER waves through the application of a 10–30-day band-pass filter (Figure S7b1 in Supporting Information S1). Meanwhile, theoretical circulation structure of MRG waves is identified in the 2–10-day filtered LTr winds (Figure S7a1 in Supporting Information S1). However, the meridional winds associated with the MRG waves do not contribute to the convective initiation.

By Dec. 05, convection intensifies in the NW-EIO and extends eastward to 70°E (Figure 4a2). An anomalous counterclockwise circulation is evident south of the convection area, centered at 50°E, just south of the equator (Figure 4b2). Strengthened LTr anomalous northeasterlies along the Somali coast and southerlies within 50°E–65°E, 5°S–4°N, drive strong meridional convergence associated with the enhanced convection west of 60°E. The anticyclonic circulation, previously identified as the southern gyre of ER waves on Dec. 02 (Figure 4c1), shifts westward to 54°E, 4°S, facilitating weak meridional convergence in the NW-EIO (Figure 4c2). Additionally, easterlies develop within 60°E−70°E, 5°N–10°N, converging with southwesterlies to extend convection eastward beyond 60°E (Figure 4b2). Sub-monthly scale winds significantly contribute to these easterlies (Figure 4c2), primarily from the 10–30-day filtered winds (Figure S7b2 in Supporting Information S1). At this time, the circulation structures in the EIO differ remarkably from those of the theoretical MRGTD and ER waves, likely due to the modulation of intensified TCs (Figure S7a2 and S7b2 in Supporting Information S1).

On Dec.08, convection extends from the NW-EIO to the C-EIO (Figure 4a3). Strengthened northeasterlies enhance the LTr anomalous circulation at 50°E, 2°S, intensifying convection east of 60°E (Figure 4b3). Strong easterlies develop north of the equator in the E-EIO as Nov. MJO weakens over the MC (Figure 4b3). These easterlies converge with southwesterlies west of 65°E, leading to intense convection around 70°E (Figure 4a3). Convection also develops east of 80°E, southwest of Sri Lanka (Figure 4a3), primarily driven by the convergence of easterlies (Figure 4b3), as indicated by their time evolution during Dec. 06–07 (Figure S8 in

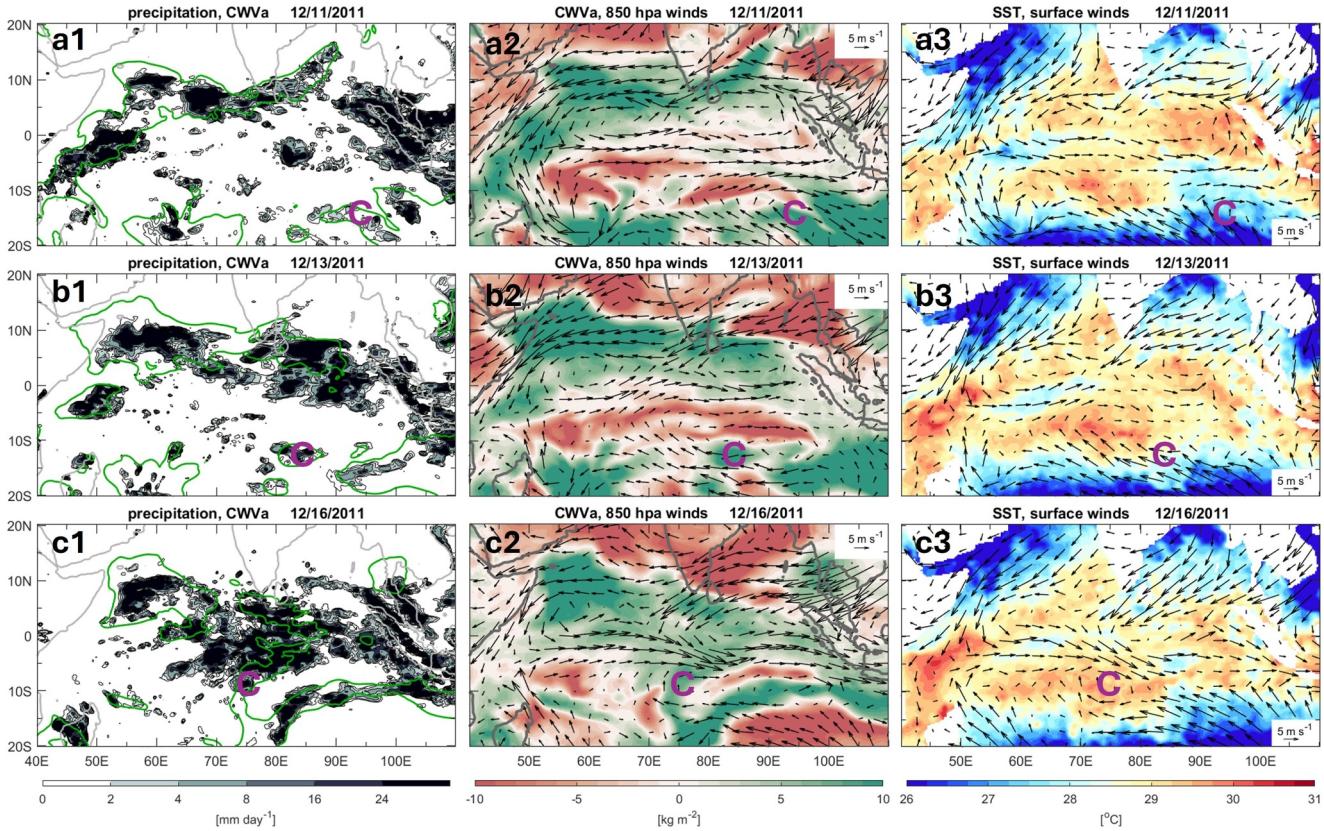

Figure 5. (a1) Precipitation (shading) and CWVa contours of 6 kg m^{-2} (green lines); (a2) CWVa (shading) and 850 hPa winds (vectors); (a3) Daily mean sea surface temperature (shading) and 10 m surface winds (vectors) on Dec. 11; (b1–b3) are the same as (a1–a3) except on Dec. 13; (c1–c3) are the same as (a1–a3) except on Dec. 16. The arrow size in the legend indicates 5 m s^{-1} for surface winds and 850 hPa winds. The cyclonic circulation of a TD-type disturbance, generated as part of the weakened eTC on Dec. 11, is marked with a letter "C" in purple at its approximate center on each day.

Supporting Information S1). Sub-monthly scale winds substantially strengthen the equatorial easterlies in the E-EIO. In addition, the anticyclonic circulation associated with the sub-monthly scale waves at 50°E on the equator, significantly contributes to the convection west of 65°E (Figure 4c3). Another anticyclonic circulation is evident at 72°E, 5°S, promoting zonal convergence and convection in the C-EIO. These circulations can be clearly identified in the 10–30-day filtered winds (Figure S7b3 in Supporting Information S1).

Previous studies suggest that the characteristics of westward-propagating equatorial waves can be significantly altered by variations in background flow (e.g., G. Chen & Huang, 2009; Dickinson & Molinari, 2002; Frank & Roundy, 2006; Fukutomi & Yasunari, 2013; Schreck et al., 2012). For the Dec. MJO event, these waves could be substantially modulated by the location and intensity of TCs, strengthened monsoon northeasterlies and convection development in the NW-EIO. While these analyses highlight the role of equatorial waves in convection development in the N-EIO, further theoretical and modeling studies are necessary to elucidate detailed processes, which are beyond the scope of this study.

3.5. Development of Large-Scale Convective System Across the Equator After TCs Dissipate and the Dec. MJO Initiation

After both TCs dissipate on Dec. 11, strong convection persists in the NW-EIO (Figure 5a1), north of a cyclonic circulation centered at 65°E, 2°N (Figure 5a2). Additionally, new convection develops in the eastern TIO, including the BOB, Sumatra, and near the equator, surrounding a cyclonic gyre centered slightly north of the equator over a warm SST area (Figures 5a2 and 5a3). These convection areas are associated with intensified northeasterlies. Consequently, a large-scale convective system is established across nearly the entire N-EIO. Strong convection also forms in the SW-EIO near the Somali coast where northeasterlies converges with southeasterlies (Figures 5a1 and 5a2). However, unlike the convection initiated in the NW-EIO, it does not

propagate further eastward due to the DAB. Moreover, a cyclonic gyre is identified around 95°E, 15°S in the wake of the substantially weakened eTC (purple markers in Figures 5a1–5a3).

On Dec. 13, the enhanced convection in the NW-EIO strengthens the counterclockwise circulation over 55°E–70°E, 5°S–8°N centered near the equator, supporting southwesterlies in the equatorial area between 65°E–75°E (Figures 5b1–5b2). These southwesterlies converge with strong northeasterlies in the C-EIO area between the two cyclonic circulations, enhancing local convection and moistening the area (Figure 5b2; Figure S9a in Supporting Information S1). Concurrently, strong convection develops in the E-EIO within the cyclonic gyre centered around 87°E, 2°N, where warm SSTs and relatively weak surface winds are observed on Dec. 11 (Figure 5a3). This leads to moistening over the equator (Figure 5b2) and SST cooling in the E-EIO (Figure 5b3). In the S-EIO, SST warms notably in the DAB region. Nevertheless, the DAB remains in a large area spanning 50°E–95°E, 15°S-Eq, despite weakened intensity. The cyclonic gyre identified on Dec. 11 propagates westward to 85°E, with convection developing at its center, indicating characteristics of a TD-type disturbance (Figures 5b1 and 5b2).

On Dec. 16, large-scale deep convective systems have extended over both hemispheres of the EIO (Figure 5c1). The northeasterlies in the BOB further intensify and generate strong convergence near the equator. In the E-EIO, the cyclonic circulation moves further equatorward with its center east to the deep convection area, promoting strong westerlies in the S-EIO (Figures 5c2 and 5c3). Meanwhile, the cyclonic gyre continues moving westward to 75°E, 10°S, south of the enhanced westerlies (Figures 5c2 and 5c3), becoming an essential part of the large-scale organized convective system (Figure 5c1). After Dec. 16, this cyclonic circulation and the one centered just north of the equator form a double-gyre circulation, generating the Dec. MJO-associated westerly wind bursts slightly south of the equator. Substantial moistening occurs over the S-EIO, driven primarily by vertical moisture advection associated with deep convection (Figure S9b in Supporting Information S1), eliminating the DAB in the C-EIO. Convection develops a hierarchical structure, characterized by multi-scale convective systems embedded within a broader convective envelope (Figures 5c2 and 5c3). Consequently, large-scale organized convection associated with the Dec. MJO is initiated at this stage (Figures S2b, S2c, S10 in Supporting Information S1).

4. Conclusions and Discussion

The MJO is the leading mode of atmospheric intraseasonal variability during boreal winter and spring, which has a profound impact on global tropical cyclone (TC) activity as demonstrated in many previous studies (e.g., Klotzbach, 2014; Zhang, 2013). Since TCs are associated with anomalous large-scale circulations, they could also influence the MJO. However, such an influence has not been reported so far. Unlike typical MJO events initiated in the TIO, where convection begins in the Southwest TIO and develops equatorward into the MJO deep convection, the convection of December 2011 MJO (Dec. MJO) develops primarily in the northern equatorial IO (N-EIO) due to the influence of two TCs in the southern TIO. This study examines the impact of TCs on the convection development leading to the Dec. MJO initiation.

Before the Dec. MJO initiation, two TCs were active in the southern TIO during Dec. 02–11, strongly modulating large-scale circulation and moisture distribution over the EIO. The anomalous circulations of TCs significantly enhance westerlies in the southern EIO (S-EIO) within 10°S-Eq. In addition, they transport dry air from subtropics to the EIO through horizontal advection, producing a DAB in the S-EIO, where the moist climatological ITCZ is located. The western part of the DAB (wDAB) is sustained by zonal advection driven by the western TC (wTC)-enhanced westerlies, along with the descent associated with wTC-induced meridional circulation. The wDAB covers the SCTR region, where cold SST anomaly is generated by the wTC-associated wind forcing, preventing convective initiation in the Southwest TIO. The eastern part of the DAB persists during the TC-active period due to drying driven by moisture sink and horizontal advection. The DAB favors convection development in the moist N-EIO, which is examined in the context of sub-monthly scale waves. These waves, primarily westward-propagating equatorial waves significantly altered by variations in background flow, largely contribute to convection initiation in the northwestern EIO and its subsequent eastward development into the central EIO (C-EIO).

After TCs dissipate, convective systems spanning nearly the entire N-EIO form associated with the strengthened northeasterlies over the Arabian Sea and the Bay of Bengal. Subsequently, SST warms notably in the S-EIO. The enhanced northeasterlies promote deep convection in the central S-EIO, eliminating DAB over this area. Meanwhile, a TD-type disturbance, generated during the weakening of the eastern TC, propagates westward into

the C-EIO. A hierarchical convective system extending over both hemispheres with multi-scale convective systems organized into a broader convective envelope is established, indicating the initiation of the Dec. MJO convection in the C-EIO.

While this study demonstrates the prominent impact of TCs in the southern TIO on the development of the December 2011 MJO, the results are based on the analysis of one case. The large-scale atmospheric and oceanic conditions prior to the MJO initiation also vary substantially from event to event (e.g., Li et al., 2015; Matthews, 2008). Moreover, the timing of TC activity relative to the MJO development could affect the MJO initiation. Although this study identified TC-linked processes that influence the development of large-scale convection, such as TC-induced atmospheric circulation and moisture distribution and air-sea interactions in the SCTR region, the relative importance of these processes is not quantified. Further analyses and modeling studies involving many cases are necessary to address these issues.

Data Availability Statement

The IBTrACS data can be accesses at https://www.ncei.noaa.gov/products/international-best-track-archive. The CMORPH precipitation data can be downloaded from https://www.ncei.noaa.gov/products/climate-data-records/precipitation-cmorph. The NOAA OISST v2 data can be downloaded at https://www.ncei.noaa.gov/products/optimum-interpolation-sst. The CCMP surface wind data are available at http://www.remss.com/measurements/ccmp/. The OLR data can be found at https://psl.noaa.gov/data/gridded/data.olrcdr.interp.html. The ERA5 data can be found at https://cds.climate.copernicus.eu/datasets/reanalysis-era5-pressure-levels?tab=overview. The DYNAMO sounding data provided by NCAR/EOL under the sponsorship of the National Science Foundation can be obtained from https://orca.atmos.washington.edu/dynamo_legacy/.

Acknowledgments
This research is supported by DOD Grants N00014-22-S-F008 and W911NF-20-1-0309, NASA OVWST Grant 80NSSC23K0982 and NSF Grant OCE 2421780. TS is also supported by NSF Grant OCE 2242194. Computing resources were partly provided by the HPC system at the Texas A&M University at College Station and Corpus Christi. The authors gratefully acknowledge the constructive comments of the three anonymous reviewers.

References

Aberson, S. D., & Kaplan, J. (2020). The relationship between the Madden–Julian Oscillation and tropical cyclone rapid intensification. *Weather and Forecasting*, *35*(5), 1865–1870. https://doi.org/10.1175/WAF-D-19-0209.1

Aiyyer, A., & Molinari, J. (2008). MJO and tropical cyclogenesis in the Gulf of Mexico and eastern Pacific: Case study and idealized numerical modeling. *Journal of the Atmospheric Sciences*, *65*(8), 2691–2704. https://doi.org/10.1175/2007JAS2348.1

Atlas, R., Hoffman, R. N., Ardizzone, J., Leidner, S. M., Jusem, J. C., Smith, D. K., & Gombos, D. (2011). A cross-calibrated, multiplatform ocean surface wind velocity product for meteorological and oceanographic applications. *Bulletin of the American Meteorological Society*, *92*(2), 157–174. https://doi.org/10.1175/2010BAMS2946.1

Balaguru, K., Leung, L. R., Hagos, S. M., & Krishnakumar, S. (2021). An oceanic pathway for Madden–Julian Oscillation influence on Maritime Continent Tropical Cyclones. *npj Climate and Atmospheric Science*, *4*(1), 52. https://doi.org/10.1038/s41612-021-00208-4

Barrett, B. S., & Leslie, L. M. (2009). Links between tropical cyclone activity and Madden–Julian Oscillation phase in the North Atlantic and Northeast Pacific basins. *Monthly Weather Review*, *137*(2), 727–744. https://doi.org/10.1175/2008MWR2602.1

Beal, L. M., Hormann, V., Lumpkin, R., & Foltz, G. R. (2013). The response of the surface circulation of the Arabian Sea to monsoonal forcing. *Journal of Physical Oceanography*, *43*(9), 2008–2022. https://doi.org/10.1175/JPO-D-13-033.1

Bessafi, M., & Wheeler, M. C. (2006). Modulation of south Indian Ocean Tropical cyclones by the Madden–Julian Oscillation and convectively coupled equatorial waves. *Monthly Weather Review*, *134*(2), 638–656. https://doi.org/10.1175/MWR3087.1

Camargo, S. J., Robertson, A. W., Barnston, A. G., & Ghil, M. (2008). Clustering of eastern North Pacific tropical cyclone tracks: ENSO and MJO effects. *Geochemistry, Geophysics, Geosystems*, *9*(6), Q06V05. https://doi.org/10.1029/2007GC001861

Chand, S. S., & Walsh, K. J. E. (2010). The influence of the Madden–Julian Oscillation on tropical cyclone activity in the Fiji region. *Journal of Climate*, *23*(4), 868–886. https://doi.org/10.1175/2009JCLI3316.1

Chen, G., & Huang, R. (2009). Interannual variations in mixed Rossby–gravity waves and their impacts on tropical Cyclogenesis over the Western North Pacific. *Journal of Climate*, *22*(3), 535–549. https://doi.org/10.1175/2008JCLI2221.1

Chen, S., Flatau, M., Jensen, T. G., Shinoda, T., Schmidt, J., May, P., et al. (2015). A study of CINDY/DYNAMO MJO suppressed phase. *Journal of the Atmospheric Sciences*, *72*(10), 3755–3779. https://doi.org/10.1175/JAS-D-13-0348.1

Dickinson, M., & Molinari, J. (2002). Mixed Rossby–gravity waves and western Pacific tropical cyclogenesis. Part I: Synoptic evolution. *Journal of the Atmospheric Sciences*, *59*(14), 2183–2196. https://doi.org/10.1175/1520-0469(2002)059<2183:MRGWAW>2.0.CO;2

Duchon, C. E. (1979). Lanczos filtering in one and two dimensions. *Journal of Applied Meteorology and Climatology*, *18*(8), 1016–1022. https://doi.org/10.1175/1520-0450(1979)018<1016:LFIOAT>2.0.CO;2

Frank, W. M., & Roundy, P. E. (2006). The role of tropical waves in tropical cyclogenesis. *Monthly Weather Review*, *134*(9), 2397–2417. https://doi.org/10.1175/MWR3204.1

Fukutomi, Y., & Yasunari, T. (2013). Structure and characteristics of submonthly-scale waves along the Indian Ocean ITCZ. *Climate Dynamics*, *40*(7–8), 1819–1839. https://doi.org/10.1007/s00382-012-1417-x

Hall, J. D., Matthews, A. J., & Karoly, D. J. (2001). The modulation of tropical cyclone activity in the Australian region by the Madden–Julian Oscillation. *Monthly Weather Review*, *129*(12), 2970–2982. https://doi.org/10.1175/1520-0493(2001)129<2970:TMOTCA>2.0.CO;2

Hansen, K. A., Janiga, M. A., Majumdar, S. J., & Kirtman, B. P. (2024). Impact of MJO propagation speed on active Atlantic Tropical Cyclone activity periods. *Geophysical Research Letters*, *51*(5), e2023GL106872. https://doi.org/10.1029/2023GL106872

Hermes, J. C., & Reason, C. J. C. (2008). Annual cycle of the South Indian Ocean (Seychelles-Chagos) thermocline ridge in a regional ocean model. *Journal of Geophysical Research*, *113*(C4), C04035. https://doi.org/10.1029/2007JC004363

Hersbach, H., Bell, B., Berrisford, P., Hirahara, S., Horányi, A., Muñoz-Sabater, J., et al. (2020). The ERA5 global reanalysis. *Quarterly Journal of the Royal Meteorological Society*, *146*(730), 1999–2049. https://doi.org/10.1002/qj.3803

Ho, C.-H., Kim, J.-H., Jeong, J.-H., Kim, H.-S., & Chen, D. (2006). Variation of tropical cyclone activity in the South Indian Ocean: El Niño–Southern Oscillation and Madden-Julian Oscillation effects. *Journal of Geophysical Research*, *111*(D22), D22101. https://doi.org/10.1029/2006JD007289

Jiang, X., Adames, Á. F., Kim, D., Maloney, E. D., Lin, H., Kim, H., et al. (2020). Fifty years of research on the Madden-Julian Oscillation: Recent progress, challenges, and perspectives. *Journal of Geophysical Research: Atmospheres*, *125*(17), e2019JD030911. https://doi.org/10.1029/2019JD030911

Johnson, R. H., & Ciesielski, P. E. (2013). Structure and properties of Madden–Julian Oscillations deduced from DYNAMO sounding arrays. *Journal of the Atmospheric Sciences*, *70*(10), 3157–3179. https://doi.org/10.1175/JAS-D-13-065.1

Johnson, R. H., Schubert, W., Taft, R., Ciesielski, P., & Kerns, B. W. (2019). *DYNAMO areal averages from observations and model data: DYNAMO legacy collection*. Version 1.0. UCAR/NCAR - Earth Observing. https://doi.org/10.26023/HEKP-RP69-CQ00

Kerns, B. W., & Chen, S. S. (2014). Equatorial dry air intrusion and related synoptic variability in MJO initiation during DYNAMO. *Monthly Weather Review*, *142*(3), 1326–1343. https://doi.org/10.1175/MWR-D-13-00159.1

Klotzbach, P. J. (2012). El Niño-Southern Oscillation, the Madden-Julian Oscillation and Atlantic basin tropical cyclone rapid intensification. *Journal of Geophysical Research*, *117*(D14), D14104. https://doi.org/10.1029/2012JD017714

Klotzbach, P. J. (2014). The Madden–Julian Oscillation's impacts on worldwide tropical cyclone activity. *Journal of Climate*, *27*(6), 2317–2330. https://doi.org/10.1175/JCLI-D-13-00483.1

Klotzbach, P. J., & Blake, E. S. (2013). North-central Pacific tropical cyclones: Impacts of El Niño–Southern Oscillation and the Madden–Julian Oscillation. *Journal of Climate*, *26*(19), 7720–7733. https://doi.org/10.1175/JCLI-D-12-00809.1

Klotzbach, P. J., Schreck, C. J., Compo, G. P., Wood, K. M., Oliver, E. C. J., Bowen, S. G., & Bell, M. M. (2023). Influence of the Madden-Julian Oscillation on continental United States hurricane landfalls. *Geophysical Research Letters*, *50*(7), e2023GL102762. https://doi.org/10.1029/2023GL102762

Knapp, K. R., Kruk, M. C., Levinson, D. H., Diamond, H. J., & Neumann, C. J. (2010). The international best track archive for climate Stewardship (IBTrACS). *Bulletin of the American Meteorological Society*, *91*(3), 363–376. https://doi.org/10.1175/2009BAMS2755.1

Krishnamohan, K. S., Mohanakumar, K., & Joseph, P. V. (2012). The influence of Madden–Julian Oscillation in the genesis of North Indian Ocean tropical cyclones. *Theoretical and Applied Climatology*, *109*(1–2), 271–282. https://doi.org/10.1007/s00704-011-0582-x

Lee, H.-T., Schreck, C. J., & Knapp, K. R. (2014). Generation of the daily OLR climate data Record. In *2014 EUMETSAT Meteorological Satellite Conference, 22-26 September 2014*.

Li, T., Zhao, C., Hsu, P., & Nasuno, T. (2015). MJO initiation processes over the tropical Indian Ocean during DYNAMO/CINDY2011. *Journal of Climate*, *28*(6), 2121–2135. https://doi.org/10.1175/JCLI-D-14-00328.1

Liebmann, B., & Hendon, H. H. (1990). Synoptic-scale disturbances near the equator. *Journal of the Atmospheric Sciences*, *47*(12), 1463–1479. https://doi.org/10.1175/1520-0469(1990)047<1463:SSDNTE>2.0.CO;2

Liebmann, B., Hendon, H. H., & Glick, J. D. (1994). The relationship between tropical cyclones of the western Pacific and Indian Oceans and the Madden-Julian Oscillation. *Journal of the Meteorological Society of Japan*, *72*(3), 401–412. https://doi.org/10.2151/jmsj1965.72.3_401

Madden, R. A., & Julian, P. R. (1971). Detection of a 40-50 day oscillation in the zonal wind in the tropical Pacific. *Journal of the Atmospheric Sciences*, *28*(5), 702–708. https://doi.org/10.1175/1520-0469(1971)028<0702:doadoi>2.0.co;2

Madden, R. A., & Julian, P. R. (1972). Description of global-scale circulation cells in the tropics with a 40–50 Day period. *Journal of the Atmospheric Sciences*, *29*(6), 1109–1123. https://doi.org/10.1175/1520-0469(1972)029<1109:DOGSCC>2.0.CO;2

Maloney, E. D., & Hartmann, D. L. (2000). Modulation of eastern north Pacific hurricanes by the Madden–Julian Oscillation. *Journal of Climate*, *13*(9), 1451–1460. https://doi.org/10.1175/1520-0442(2000)013<1451:MOENPH>2.0.CO;2

Matsuno, T. (1966). Quasi-geostrophic motions in the equatorial area. *Journal of the Meteorological Society of Japan*, *44*(1), 25–43. https://doi.org/10.2151/jmsj1965.44.1_25

Matthews, A. J. (2008). Primary and successive events in the Madden–Julian Oscillation. *Quarterly Journal of the Royal Meteorological Society*, *134*(631), 439–453. https://doi.org/10.1002/qj.224

Moum, J. N., de Szoeke, S. P., Smyth, W. D., Edson, J. B., DeWitt, H. L., Moulin, A. J., et al. (2014). Air–Sea interactions from westerly wind bursts during the November 2011 MJO in the Indian Ocean. *Bulletin of the American Meteorological Society*, *95*(8), 1185–1199. https://doi.org/10.1175/bams-d-12-00225.1

Muraleedharan, P. M., Prasanna Kumar, S., Mohana kumar, K., Sijikumar, S., Sivakumar, K. U., & Mathew, T. (2015). Observational evidence of Mixed Rossby Gravity waves at the central equatorial Indian Ocean. *Meteorology and Atmospheric Physics*, *127*(4), 407–417. https://doi.org/10.1007/s00703-015-0376-2

Powell, S. W., & Houze, R. A. (2015). Effect of dry large-scale vertical motions on initial MJO convective onset. *Journal of Geophysical Research: Atmospheres*, *120*(10), 4783–4805. https://doi.org/10.1002/2014JD022961

Ramsay, H. A., Camargo, S. J., & Kim, D. (2012). Cluster analysis of tropical cyclone tracks in the Southern Hemisphere. *Climate Dynamics*, *39*(3–4), 897–917. https://doi.org/10.1007/s00382-011-1225-8

Reynolds, R. W., Smith, T. M., Liu, C., Chelton, D. B., Casey, K. S., & Schlax, M. G. (2007). Daily high-resolution-blended analyses for sea surface temperature. *Journal of Climate*, *20*(22), 5473–5496. https://doi.org/10.1175/2007JCLI1824.1

Roundy, P. E., & Frank, W. M. (2004). A climatology of waves in the equatorial region. *Journal of the Atmospheric Sciences*, *61*(17), 2105–2132. https://doi.org/10.1175/1520-0469(2004)061<2105:ACOWIT>2.0.CO;2

Ruppert, J. H., & Johnson, R. H. (2015). Diurnally modulated cumulus moistening in the preonset stage of the Madden–Julian Oscillation during DYNAMO. *Journal of the Atmospheric Sciences*, *72*(4), 1622–1647. https://doi.org/10.1175/JAS-D-14-0218.1

Rydbeck, A. V., & Jensen, T. G. (2017). Oceanic Impetus for convective onset of the Madden–Julian Oscillation in the western Indian Ocean. *Journal of Climate*, *30*(11), 4299–4316. https://doi.org/10.1175/JCLI-D-16-0595.1

Schreck, C. J., Molinari, J., & Aiyyer, A. (2012). A global view of equatorial waves and tropical cyclogenesis. *Monthly Weather Review*, *140*(3), 774–788. https://doi.org/10.1175/MWR-D-11-00110.1

Shinoda, T., Han, W., Zamudio, L., Lien, R.-C., & Katsumata, M. (2017). Remote ocean response to the Madden–Julian Oscillation during the DYNAMO field campaign: Impact on Somali current system and the Seychelles–Chagos Thermocline Ridge. *Atmosphere*, *8*(9), 171. https://doi.org/10.3390/atmos8090171

Shinoda, T., Jensen, T. G., Flatau, M., & Chen, S. (2013). Surface wind and upper ocean variability associated with the Madden-Julian Oscillation simulated by the Coupled Ocean-Atmosphere Mesoscale Prediction System (COAMPS). *Monthly Weather Review*, *141*(7), 2290–2307. https://doi.org/10.1175/MWR-D-12-00273.1

Sobel, A. H., & Maloney, E. D. (2000). Effect of ENSO and the MJO on western North Pacific tropical cyclones. *Geophysical Research Letters*, *27*(12), 1739–1742. https://doi.org/10.1029/1999GL011043

Takasuka, D., Kohyama, T., Miura, H., & Suematsu, T. (2021). MJO initiation triggered by amplification of upper-tropospheric dry mixed Rossby-gravity waves. *Geophysical Research Letters*, *48*(20), e2021GL094239. https://doi.org/10.1029/2021GL094239

Takasuka, D., & Satoh, M. (2020). Dynamical roles of mixed Rossby–gravity waves in driving convective initiation and propagation of the Madden–Julian Oscillation: General views. *Journal of the Atmospheric Sciences*, *77*(12), 4211–4231. https://doi.org/10.1175/JAS-D-20-0050.1

Takasuka, D., Satoh, M., & Yokoi, S. (2019). Observational evidence of mixed Rossby-gravity waves as a driving force for the MJO convective initiation and propagation. *Geophysical Research Letters*, *46*(10), 5546–5555. https://doi.org/10.1029/2019GL083108

Ventrice, M. J., Thorncroft, C. D., & Roundy, P. E. (2011). The Madden–Julian Oscillation's influence on African easterly waves and downstream tropical cyclogenesis. *Monthly Weather Review*, *139*(9), 2704–2722. https://doi.org/10.1175/MWR-D-10-05028.1

Webber, B. G. M., Matthews, A. J., & Heywood, K. J. (2010). A dynamical ocean feedback mechanism for the Madden–Julian Oscillation. *Quarterly Journal of the Royal Meteorological Society*, *136*(648), 740–754. https://doi.org/10.1002/qj.604

Webber, B. G. M., Matthews, A. J., Heywood, K. J., & Stevens, D. P. (2012). Ocean Rossby waves as a triggering mechanism for primary Madden–Julian events. *Quarterly Journal of the Royal Meteorological Society*, *138*(663), 514–527. https://doi.org/10.1002/qj.936

Wentz, F. J., Scott, J., Hoffman, R., Leidner, M., Atlas, R., & Ardizzone, J. (2015). *Remote Sensing Systems Cross-Calibrated Multi-Platform (CCMP) 6-hourly ocean vector wind analysis product on 0.25 deg grid, Version 2.0*. Remote Sensing System.

West, B. J., Han, W., Zhang, L., & Li, Y. (2020). The role of oceanic processes in the initiation of boreal winter intraseasonal oscillations over the Indian Ocean. *Journal of Geophysical Research: Oceans*, *125*(2), e2019JC015426. https://doi.org/10.1029/2019JC015426

Xie, P., Joyce, R., Wu, S., Yoo, S.-H., Yarosh, Y., Sun, F., & Lin, R. (2019). *NOAA CDR Program (2019): NOAA Climate Data Record (CDR) of CPC Morphing Technique (CMORPH) high resolution global precipitation Estimates, version 1*. NOAA National Centers for Environmental Information.

Xie, S.-P., Annamalai, H., Schott, F. A., & McCreary Jr, J. P. (2002). Structure and mechanisms of south Indian Ocean climate variability. *Journal of Climate*, *15*(8), 864–878. https://doi.org/10.1175/1520-0442(2002)015<0864:SAMOSI>2.0.CO;2

Yanai, M., Esbensen, S., & Chu, J. (1973). Determination of bulk properties of tropical cloud clusters from large-scale heat and moisture budgets. *Journal of the Atmospheric Sciences*, *30*(4), 611–627. https://doi.org/10.1175/1520-0469(1973)030<0611:DOBPOT>2.0.CO;2

Yasunaga, K., Yoneyama, K., Moteki, Q., Fujita, M., Takayabu, Y. N., Suzuki, J., et al. (2010). Characteristics of 3–4- and 6–8-day period disturbances observed over the tropical Indian Ocean. *Monthly Weather Review*, *138*(11), 4158–4174. https://doi.org/10.1175/2010MWR3469.1

Yoneyama, K., Zhang, C., & Long, C. N. (2013). Tracking pulses of the Madden–Julian Oscillation. *Bulletin of the American Meteorological Society*, *94*(12), 1871–1891. https://doi.org/10.1175/BAMS-D-12-00157.1

Zhang, C. (2013). Madden–Julian Oscillation: Bridging weather and climate. *Bulletin of the American Meteorological Society*, *94*(12), 1849–1870. https://doi.org/10.1175/BAMS-D-12-00026.1

Zhao, C., Li, T., & Zhou, T. (2013). Precursor signals and processes associated with MJO initiation over the tropical Indian Ocean. *Journal of Climate*, *26*(1), 291–307. https://doi.org/10.1175/JCLI-D-12-00113.1